Evaluation of the diffusion coefficient of fluorine during the electropolishing of niobium

Hui Tian[*] and Charles E. Reece

Thomas Jefferson National Accelerator Facility, Newport News, Virginia 23606, USA
(Received 30 November 2009; published 25 August 2010)

Future accelerators require unprecedented cavity performance, which is strongly influenced by interior surface nanosmoothness. Electropolishing (EP) is the technique of choice being developed for high-field superconducting radio frequency (SRF) cavities. Previous study has shown that the mechanism of Nb electropolishing proceeds by formation and dissolution of a compact salt film under fluorine diffusion-limited mass transport control. We pursue an improved understanding of the microscopic conditions required for optimum surface finishing. The viscosity of the standard electrolyte has been measured using a commercial viscometer, and the diffusion coefficient of fluorine was derived at a variety of temperatures from 0 to 50°C using a Nb rotating disk electrode. In addition, data indicate that electrode kinetics becomes competitive with the mass transfer current limitation and increases dramatically with temperature. These findings are expected to guide the optimization of EP process parameters for achieving controlled, reproducible, and uniform nanosmooth surface finishing of SRF cavities.

PACS numbers: 82.45.Rr, 82.80.Fk, 81.65.Ps

I. INTRODUCTION

Superconducting radio frequency (SRF) cavities have become the principal building blocks for charged particle accelerators. The unique characteristics of SRF materials allow them to support very high electromagnetic fields on their surfaces with minimal parasitic heat dissipation when cooled to low temperatures, typically ~2 K. New applications of SRF cavities are forthcoming for some of science's grandest instruments, such as Jefferson Lab's Continuous Electron Beam Accelerator Facility and its 12 GeV upgrade now in progress, an envisioned electron ion collider, the Facility for Rare Isotope Beams, the International Linear Collider (ILC), proton-proton colliders, x-ray free electron lasers, storage ring light sources, linac-based light sources, energy recovery linacs, muon storage rings for neutrino sources, and eventually perhaps a high energy muon collider. These research tools are opening or will open new scientific frontiers, offering opportunities for revolutionary scientific breakthroughs.

Essential to the proper function of SRF accelerator cavities is obtaining pure, clean, and smooth interior surfaces, given that only the topmost 40–50 nm layer is directly involved with the rf fields. Controlling the creation and preservation of this finished surface is paramount. Electropolishing (EP) is the technique of choice being developed for high-field SRF cavities. With routine operation of EP facilities in recent years, more multicell SRF cavity test data have become available. Cavity performance variability has emerged as a major challenge for electropolishing processed niobium cavities [1,2], especially for the ILC, the application potential most visible

to the public, with 16 000 nine-cell cavities intended to perform at historically high acceleration gradient (> 31 MV/m). One outstanding variability issue is the unpredictable onset of field emission. Another is the quench field, which has been observed to vary unpredictably in electropolished cavities in the absence of field emission. Ongoing progress against field emission relies on elimination of surface adhering particles by improved cleanliness and high pressure rinsing. Quenches without x-ray emission are usually associated with defects: foreign material inclusions, weld beads, etch pits, and mechanical damages are severe examples. At present, besides reducing the incidence of severe defect-induced quenches via improved quality control of manufacturing practice, a complete understanding of process parameters and adequate process control are very important to help achieve reproducible high gradient cavities.

Electropolishing is a surface finishing process based on anodic dissolution of a metal or alloy in an appropriately chosen electrolyte [3]. It is characterized by the elimination of microroughness (leveling) and the absence of crystallographic and grain boundary attack (brightening) and results in the production of smooth, bright surfaces [4,5]. Leveling results from the fact that protruding parts of a rough surface dissolve faster than recessed parts. This can be achieved under either Ohmic or mass transport control [5]. Brightening can only occur under mass transport control, which suppresses crystallographic etching [5–7]. The supply and removal of reactant and product contribute to three different forms of mass transport: (i) diffusion, defined as the movement of species due to concentration gradient; (ii) convection, in which the movement is due to external mechanical energy—for example, electrode rotation or density variation; and (iii) migration movement due to a potential gradient—that is, only charged species

---
[*]Corresponding author.
huit02@jlab.org

are affected [8]. The EP process typically now applied to cavities was inherited from Siemens Co. in the 1970s [9] and was further developed by KEK in collaboration with Nomura Plating [10]. Typically, a mixture of hydrofluoric (46%–49%) and sulfuric acids (95%–98%) by volume ratio of 1:9 or 1:10 is used with a temperature range of 30–45°C measured at the cavity surface, for example, the horizontal EP in Jefferson Lab and Deutsches Elektronen Synchrotron, or in the electrolyte, for example, the High Energy Accelerator Research Organization (commonly known as KEK) EP facility, a current density of 30–100 mA/cm², and an applied cell voltage of typically 10–20 V. The surface area ratio of the niobium cavity (anode) to the typical high purity aluminum tube cathode is 10:1 during practical cavity EP processing of cylindrically symmetric multicell Nb SRF cavities.

Past cavity EP studies done on niobium SRF cavities have shown that the best polishing condition occurs in the current-limited plateau of the polarization curves. Parameters such as electrolyte temperature, acid concentration, viscosity, and stirring have strong effects on the EP process [11]. Some studies conducted on either small samples or half-cells tried to evaluate the influence of each parameter [12]. However, the application of electrochemical techniques is needed for the development of a clear picture of the exact role of each parameter involved during the EP process.

In our previous study, electrochemical impedance spectroscopy and related techniques point to the electropolishing mechanism of Nb in a sulphuric and hydrofluoric acid electrolyte as the growth and dissolution of a compact surface salt film, presumed to be Nb_2O_5, under the diffusion-limited mass transport control of fluoride and its related ions [13]. However, a detailed understanding of the diffusion of fluorine and a parametrization of resulting surface finishing control is still missing.

Rotating disk electrode (RDE) techniques are frequently used in electrochemical kinetic experiments to establish specific momentum and mass transfer characteristics [8,14,15]. RDE takes the form of a ∼5 mm diameter polished disk surrounded by an insulation sheath on all the sides except one exposed face. The structure is rotated rapidly about an axis perpendicular to the surface of the disk electrode; this movement of rotation creates a well-defined solution flow pattern as illustrated in Fig. 1 [8,14], in which the mass transport of limiting species is deliberately dominated by convection [8,14]. This property allows the RDE to be used to calculate parameters related to mass transport, such as the diffusion coefficient of various electroactive species. The hydrodynamics of the RDE system have been solved analytically by assuming spatially constant transport properties [16]. By solving the convective diffusion equation with the boundary conditions of the hydrodynamic velocity profile, the Levich equation [Eq. (1)] can be used to describe the relationship of limiting
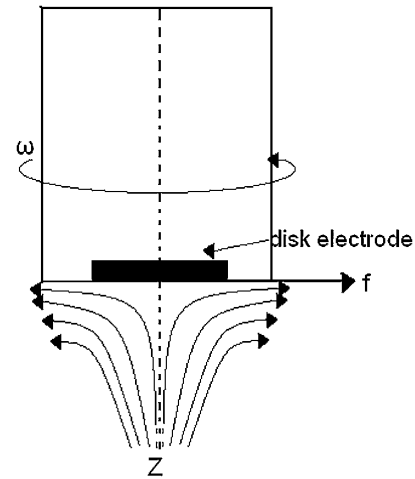

FIG. 1.   Solution movement caused by rotation of an RDE [8].

current density j_L, to the physical properties of the electrolyte bath [7,17–20]:

$$j_L = 0.62nFD^{0.67}\nu^{-0.166}c\omega^{0.5}. \quad (1)$$

Here, j_L is the limiting current density contributed by convective diffusion only, n is the number of electrons involved in electrode reaction (for fluoride and its related ions n equals 1), F is the Faraday constant, 96 485 Cmol⁻¹, ν is the kinematic viscosity in $m^2 s^{-1}$, c is the concentration of electroactive species in bulk solution in $mol.m^{-3}$ (the concentration of fluoride in 1:10 HF/H_2SO_4 studied here is 2670 mol m⁻³), and ω is the rotation speed in $rad\, s^{-1}$. Note that

$$\text{slope } (j_L \text{ vs } \omega^{0.5}) = 0.62nFD^{0.67}\nu^{-0.166}c. \quad (2)$$

Hence, a test for pure mass transport control is that the plot of j_L vs $\omega^{0.5}$ is linear and passes through the origin [21]. The corresponding diffusion coefficient D ($m^2 s^{-1}$) can then be determined when the kinematic viscosity of electrolyte and mass limited species concentration are known. The kinematic viscosity of a fluid is simply the dynamic viscosity divided by its density. We measured the density of the electrolyte in this study to be 1760 kg/m³. Table I

TABLE I. The measured dynamic viscosity of 1:10 HF/H_2SO_4 electrolyte and calculated diffusion coefficient of fluorine at 1°C, 9°C, 19°C, 30°C, 41°C, and 50°C.

Temperature (°C)	Dynamic viscosity[a] (cP)	Diffusion coefficient (m^2/s)
1	45	2.69×10^{-12}
9	38	4.86×10^{-12}
19	29	8.77×10^{-12}
30	22	1.29×10^{-11}
41	20	2.83×10^{-11}
50	18	2.90×10^{-11}

[a]The dynamic viscosity was calibrated against reference standard with and without guardleg in place.
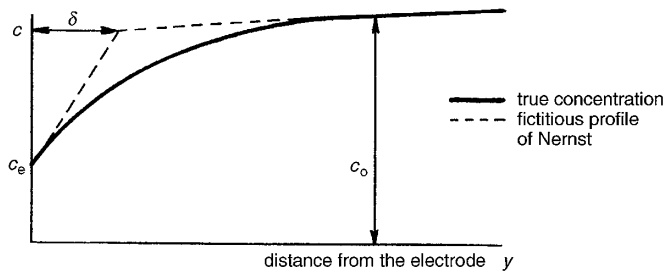
FIG. 2. Representation of the Nernst diffusion layer profile model [8].

lists the measured dynamic viscosity, and calculated diffusion coefficient of fluorine in the EP solution under different temperatures.

According to the Nernst diffusion layer model, the electrolyte can be divided into two zones (see Fig. 2) [8]. The first region is closest to the surface of the electrode with the thickness δ, which is named the Nernst diffusion layer, where it is assumed that the fluid is totally stagnant and thereby diffusion is the only mode of mass transport. In the second region outside the Nernst diffusion layer, a strong convection occurs and all species concentrations are considered as constant. The model thus assumes a concentration profile perpendicular to an electrode surface corresponding to the dotted straight lines of Fig. 2. The thickness δ of this layer is called the effective (or equivalent) thickness of the diffusion layer. Its definition is apparent from Fig. 2. It is the thickness which the diffusion layer would have if the concentration profile were a straight line coinciding with the tangent to the true concentration profile at the interface, and that straight line were extended up to the point where the bulk concentration is reached. The diffusion-limited current density is then given by [8]

$$J_l = nFDc/\delta. \qquad (3)$$

So, for a given diffusion-limited current density, fluorine concentration, and measured diffusion constant, one can calculate the effective thickness of the diffusion layer.

Recent studies for different composition of hydrofluoric and sulfuric acid electrolytes done by Fabien Éozénou et al. suggested that the diffusion coefficient of fluorine is lower in the aged mixtures by assuming the concentration of fluorine was constant [22]. In this study, we report determination of the diffusion coefficient of fluoride and its related ions in 1:10 mixture of EP solution using a Nb rotating disk electrode at different temperatures. The thickness of the Nernst diffusion layer at different temperatures was determined, and those values were used to explore the optimization of EP process parameters for achieving uniform nanosmooth surface finishing.

II. EXPERIMENTAL STUDIES

RDE experiments were performed on high purity polycrystalline Nb disk electrode samples with a reactive surface area of 0.19 cm^2. The Nb disks were mechanically polished up to 4000 grit emery paper, ultrasonically rinsed with distilled water and isopropanol, and air dried. A high purity Al wire was used as the counterelectrode. A Gamry RDE710 rotating disk electrode setup was used for the experiments with each sample mounted in a Teflon holder. The reference electrode was a saturated mercury/mercurous sulphate electrode (MSE). The electrolytes were prepared from analytic grade 49% hydrofluoric (J. T. Baker) and 96% sulphuric acid (J. T. Baker) with the volume ratio of 1:10.

The polarization curves were measured stepwise (step size $= 0.1$ volts, dwell time $= 0.25$ second) over the potential range from 0 to 22 volts. The potential between the Nb electrode and the reference electrode was recorded using a Keithley 6517A electrometer. The addition of the reference electrode allows monitoring of the potentials on the cathode and anode independently. The current was recorded with a Keithley 2000 multimeter. Prior to the polarization measurements, the electrodes were immersed in the electrolyte in an open circuit condition for 3 to 5 minutes. In order to maintain a stable temperature during the measurement, the electrochemical cell was immersed in a water bath with constant circulation of controlled proportions of hot ($\sim 70°C$), cold ($\sim 15°C$), and ice water ($\sim 0°C$). Two thermocouples were used to monitor the temperature of the electrolyte. One was placed midway between the anode and cathode to record the temperature of the bulk electrolyte, the other was positioned inside of the water bath.

The electrolyte viscosities were measured at different temperatures with a Brookfield $DV - II + PRO$ digital viscometer without stainless steel guardleg. The dynamic viscosity was calibrated against a viscosity standard. The variation of repeated viscosity measurements was about 1.5%. The electrolyte density was measured by weighing the electrolyte in a Teflon volumetric flask. The reported diffusion coefficients were verified by repeated experiments, with typical variations in limiting current densities of about 2%.

III. EXPERIMENTAL RESULTS AND DISCUSSIONS

Figure 3 shows anode polarization curves of an Nb disk electrode for 1:10 volume ratio of HF and H$_2$SO$_4$ electrolyte at different angular velocities at 9°C. The same anode polarization curves have been also obtained at the other temperatures studied here, such as 1°C, 19°C, 30°C, 41°C, and 50°C. The electrolyte temperature during the measurement was regulated within 50°C. All the polarization curves exhibit a well-defined and wide potential range of
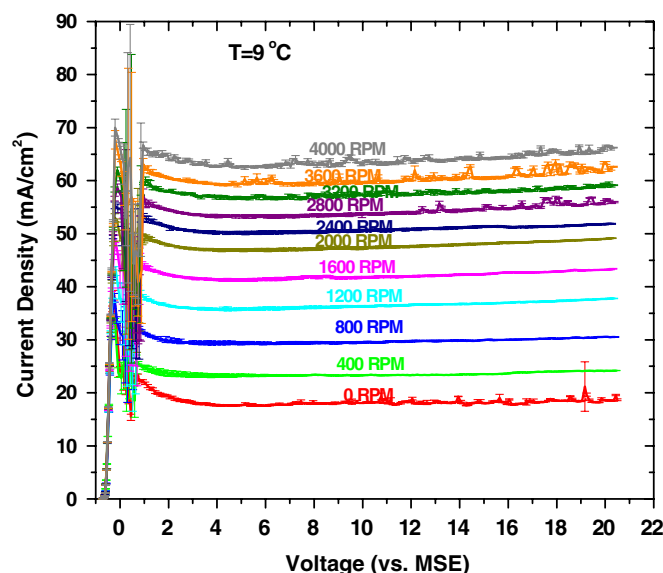
FIG. 3. (Color) The anode polarization curves of Nb RDE in 1:10 volume ratio HF and H_2SO_4 at 9°C.

FIG. 5. (Color) The limiting current density of Nb disk electrode in 1:10 volume ratio HF and H_2SO_4 plotted as a function of the square root of rotation rate at a potential 8.5 V (vs MSE).

limiting current density plateau. In this range the current is independent of the polarization voltage.

Figure 4 shows how the limited current density varies with the different RDE angular velocities at 19°C. Similar measurements were made under the other controlled temperature conditions. Figure 5 shows the typical dependence of the limiting current density on the square root of RDE rotation rate [23]. The variation of the limiting current density shows a linear behavior with respect to $\omega^{1/2}$, which provides distinct evidence that the supply of reactant, such as F ion or its related species (HF^- or HF [15]), is under mass transport control in a media with uniform viscosity.

However, the nonzero offsets at the higher electrolyte temperatures indicate the presence of an electrode kinetic mechanism; we assume it to be an electrochemical etching process that proceeds in parallel with the diffusion-limited mass transport and note that its contribution to the plateau current increases dramatically with electrolyte temperature.

In this study, J_L is determined by subtracting the non-zero offsets in Fig. 5 from the measured limiting current density under static condition at 8.5 V anode potential for different temperature electrolytes studied here. The calculated Nernst diffusion layer thickness according to Eq. (3)
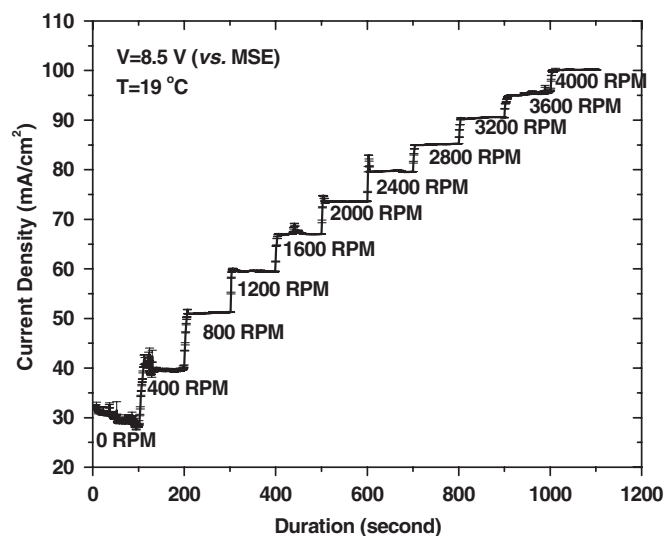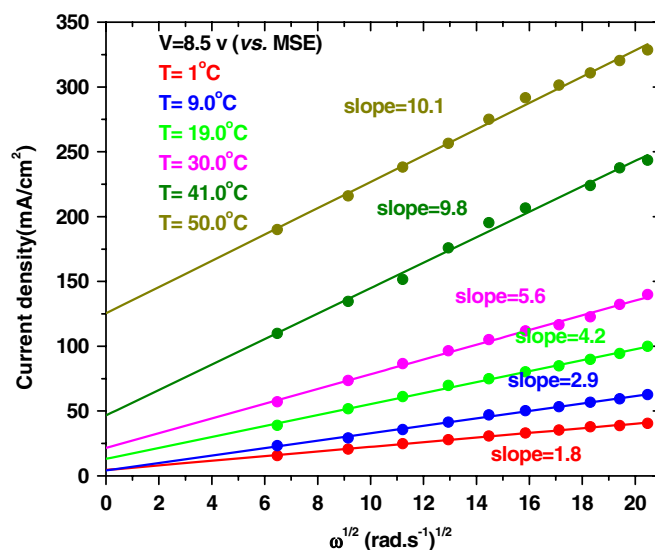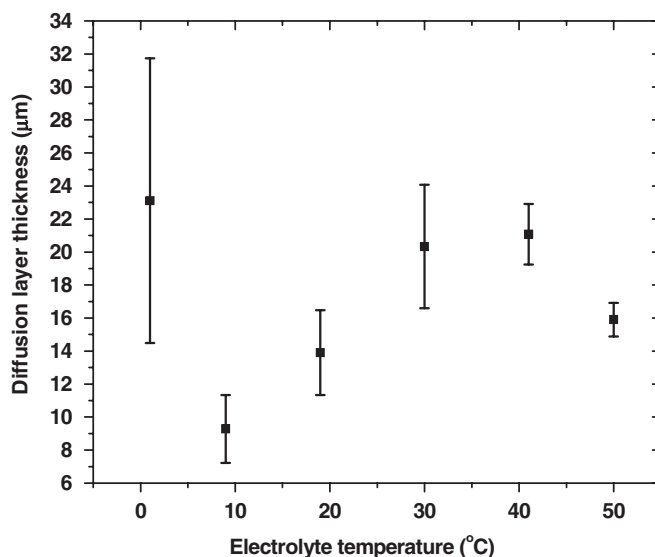

FIG. 4. The variation of limiting current density of Nb disk electrode with different rotation rate in 1:10 volume ratio HF and H_2SO_4 at 19°C at a potential 8.5 V (vs MSE).

FIG. 6. The effective Nernst diffusion layer thickness of fluorine in 1:10 volume ratio HF and H_2SO_4 during diffusion EP of niobium at the different temperatures.

is shown in Fig. 6. The uncertainty of the Nernst diffusion layer thickness determination under each temperature mostly comes from the variations of the diffusion-limited current density and the uncertainty of subtraction of the offset (especially for the low temperature, such as 1°C). Note that the Nernst diffusion layer thickness is maintained about 10–20 μm over the temperature range 1–50°C for the electrolyte studied here. At this time, we offer no interpretation for the temperature dependence of Nernst diffusion layer suggested by these data. However, it is important for our application to understand that it is the concentration gradient on the scale of δ that is expected to produce the most optimum leveling effect.

Figures 7(a) and 7(b) show atomic force microscopy (AFM) topography of two Nb samples centrifugal barrel polished (CBP) by KEK. We label them as rough CBP and

fine CBP according to the different sizes of polishing media and the different durations used. The details of treatment can be found in Ref. [24]. AFM measurements were performed using a commercial AFM (Digital Instruments: Nanoscope IV) in a tapping mode using silicon tips with a diameter of 10 nm. The samples were scanned in five different regions. The value of surface roughness was taken from the average of those five different positions for each of the samples. The AFM images were captured as arrays of height values with 512×512 points.

The AFM results in 50 μm $\times$ 50 μm scanning area show that the rough CBP treated sample has 890 $\pm$ 32 nm average surface mean square root roughness (R_q), and the average surface variation (R_z) is above 5.3 μm. Correspondingly, R_q is 178 $\pm$ 32 nm and R_z is about

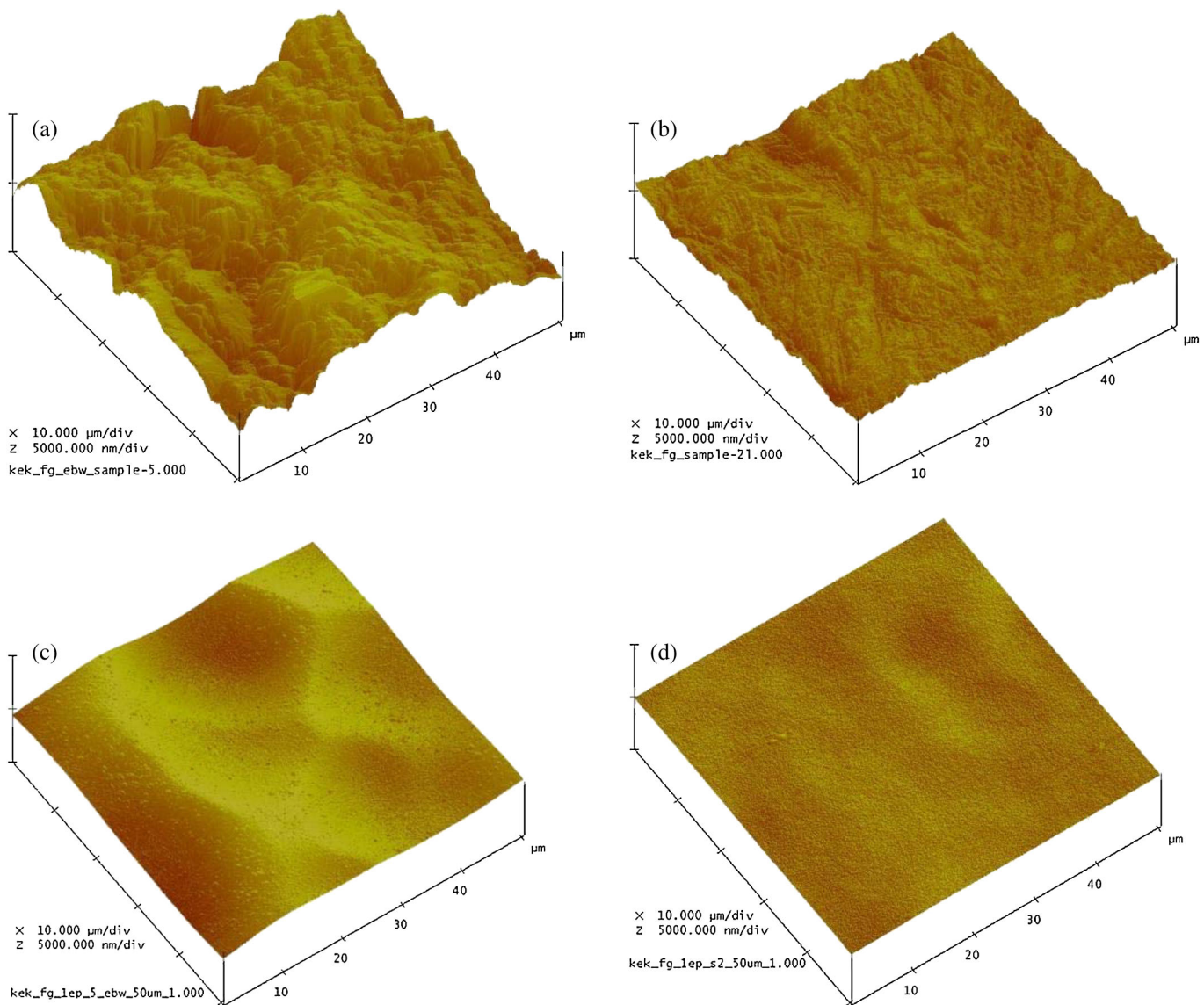FIG. 7. (Color) AFM images of CBP polycrystalline Nb samples before and after 100 min of electropolishing at 30 $\pm$ 1°C with 14 V applied cell voltage: (a) rough CBP, (b) fine CBP, (c) rough CBP after electropolishing, and (d) fine CBP after electropolishing.

HUI TIAN AND CHARLES E. REECE

Phys. Rev. ST Accel. Beams **13,** 083502 (2010)

1.6 μm for the fine CBP sample. After 100 min of EP polishing (30 μm removal) by 1:10 volume ratio HF/H$_2$SO$_4$ at 30 $\pm$ 1°C with 14 volts applied cell voltage with cathode/anode area ratio of 2:1, the fine CBP surface achieves a better finish, with 55 $\pm$ 5 nm mean square root roughness [see Fig. 7(d)], and the surface variation is about 150 nm, as compared with the rough CBP, where R_q is 187 $\pm$ 22 nm and R_z is about 1.6 μm [Fig. 7(c)]. These results give strong evidence that diffusion-limited mass transfer would produce the nanosmooth surface finishing. Further refinement of the polishing analysis as a function of temperature is planned in the near future.

Figure 8 shows the power spectral density (PSD) analysis results of fine CBP treated polycrystalline, large grain, and single crystal Nb samples with 100 min EP at 30–1°C with 14 volts applied cell voltage with cathode/anode area ratio of 2:1. The PSD-based description of surfaces was recently developed for Nb surface topography study under cavity production conditions [25–27]. It is a method of combining the measurements from different diagnostic instruments, and also reducing instrumental effects when one measures parameters such as surface roughness and correlation length [28,29]. PSD represents the spatial-frequency spectrum of surface roughness measured in inverse-length units. Briefly, a series of AFM and stylus profilometry scans are obtained from several surface locations of the specimens according to the protocol developed, and the squares of the Fourier transforms of the measured surface heights are combined as a plot of roughness PSD versus spatial frequency (inverse of wavelength). The PSD analysis in Fig. 9 shows that fine CBP produces a very reproducible surface for polycrystalline, large grain, and single crystal Nb. However, after 100 min EP at 30–1°C, a noticeable difference was observed from the different crystalline Nb samples. Compared with fine grain Nb samples, the single crystal sample shows the smallest amplitude of PSD and better correlation length. We explain the difference as perhaps caused by electrochemical etching occurring in parallel with the desired EP brightening process at the regulated 30°C condition, as suggested by the nonzero offset in the current density vs square root of rotation rate curves. If the interpretation is correct, one would anticipate a reduction in material dependent topography as the EP process temperature is lowered. Further studies will test this hypothesis.

IV. CONCLUSION

In this study, Nb electropolishing was studied using a rotating disk electrode in a 1:10 volume ratio of HF/H$_2$SO$_4$ electrolyte at different temperatures. The limiting current density demonstrates a clear dependence on fluorine diffusive mass transport. However, a parallel electrode kinetics process has been identified and it strongly depends on temperature. This suggests that high temperature may activate an etching process that recognizes different grain orientations, resulting in a nonuniform surface finishing instead of brightening. The viscosity of the standard HF/H$_2$SO$_4$ electrolyte was measured and found to strongly depend on the electrolyte temperature. The analysis yields an effective diffusion coefficient for fluoride ion on the order of 10^{-12}–10^{-11} m^2 s^{-1} under the temperatures studied, yielding a Nernst diffusion layer thickness of 10–20 μm. This study is expected to improve the fundamental understanding needed to guide the optimization of EP of niobium for SRF cavities required for particle accelerators.
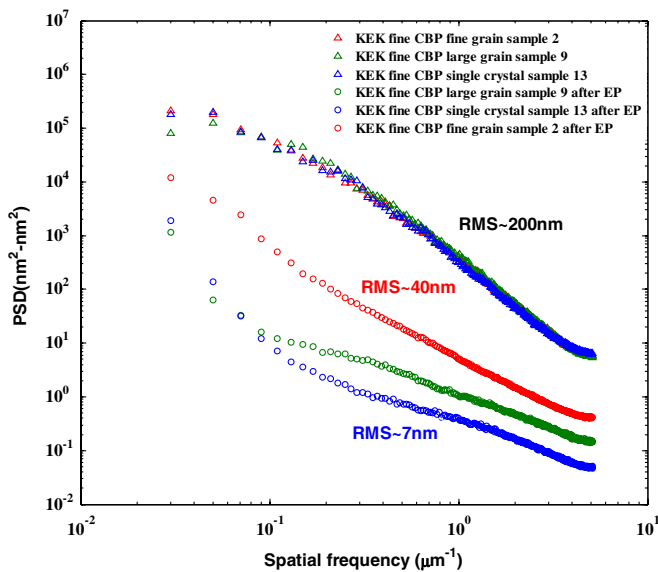
FIG. 8. (Color) The PSD of fine CBP polycrystalline, large gain and single crystal Nb samples after 30 μm removal by EP at 30 $\pm$ 1°C with 14 V applied cell voltage.

[1] C. Ginsburg, http://ilcagenda.linearcollider.org/conferenceDisplay.py?confId=1855.
[2] R. L. Geng, Jefferson Lab Internal Report.
[3] W. G. Cochran, Proc. Cambridge Philos. Soc. **30**, 365 (1934).
[4] R. Sautebin, H. Froidevaux, and D. Landolt, J. Electrochem. Soc. **127**, 1096 (1980).
[5] D. Landolt, Electrochim. Acta **32**, 1 (1987).
[6] H. Abrams and C. L. Mantell, Electrochem. Technol. **5**, 287 (1967).

[7] M. Matlosz, S. Magaino, and D. Landolt, J. Electrochem. Soc. **141**, 410 (1994).

[8] A. J. Bard and L. R. Faulkner, *Electrochemical Methods* (Wiley, New York, 1980).

[9] H. Diepers, O. Schmidt, H. Martens, and F. S. Sun, Phys. Lett. A **37**, 139 (1971).

[10] K. Saito, Y. Kojima, T. Furuya, S. Mitsonobu, S. Noguchi, K. Hosoyama, T. Nakazato, T. Tajima, K. Asano, K. Inoue, Y. Iino, H. Nomura, and K. Takeuchi, in *Proceedings of the 4th Workshop on RF Superconductivity* (KEK, Tsukuba, Japan, 1989), Vol. 2, p. 635.

[11] V. Palmieri, in Proceedings of the 11th SRF Workshop (DESY, Travemünde/Lübeck, Germany, 2003), WeT02 [http://srf2003.desy.de/fap/].

[12] F. Eozénou, A. Aspart, C. Antoine, and B. Maliki, CARE Report No. 06-10-SRF, 2006.

[13] H. Tian, S. G. Corcoran, C. E. Reece, and M. J. Kelley, J. Electrochem. Soc. **155**, D563 (2008).

[14] R. N. Adams, *Electrochemistry at Solid Electrodes* (Dekker, New York, 1969).

[15] S. Cattaria, M. Masiani, and B. Tribollet, J. Electrochem. Soc. **149**, B457 (2002).

[16] R. Sautebin and D. Landolt, J. Electrochem. Soc. **129**, 946 (1982).

[17] V. G. Levich, *Physicochemical Hydrodynamics* (Prentice-Hall, New York, 1962).

[18] R. Vidal and A. C. West, J. Electrochem. Soc. **142**, 2689 (1995).

[19] B. Du and I. I. Suni, J. Electrochem. Soc. **151**, C375 (2004).

[20] B. Du and I. I. Suni, J. Appl. Electrochem. **34**, 1215 (2004).

[21] J. H. Han, A. Bowen, T. N. Andryushchenko, R. P. Chalupa, A. E. Miller, H. S. Simka, K. C. Cadien, and S. Shankar, J. Appl. Electrochem. **38**, 1 (2007).

[22] F. Éozénou, S. Berry, Y. Gasser, and J-P. Charrier, in *14th International Conference on RF Superconductivity* (HZB, Berlin, Germany, 2009), THPPO069 [http://accelconf.web.cern.ch/AccelConf/srf2009/index.htm].

[23] J. L. Hudson and T. T. Tsotsis, Chem. Eng. Sci. **49**, 1493 (1994).

[24] T. Higuchi, K. Saito, Y. Yamazaki, T. Ikeda, and S. Ohgushi, in *Proceedings of the 10th Workshop on RF Superconductivity* (KEK, Tsukuba, Japan, 2001), p. 279.

[25] H. Tian, G. Ribeill, M. J. Kelley, and C. E. Reece, in *Proceedings of the 13th SRF Workshop* (Beijing University, Beijing, China, 2007), WEP04 [http://web5.pku.edu.cn/srf2007/proceeding.html].

[26] H. Tian, Ph.D. dissertation, Department of Applied Science, College of William and Mary, 2008.

[27] H. Tian, C. E. Reece, and M. J. Kelley (unpublished).

[28] J. Ferré-Borrull, A. Duparré, and E. Quesnel, Appl. Opt. **40**, 2190 (2001).

[29] O. Vatel, Jpn. J. Appl. Phys. **32**, 5671 (1993).